NUMERICAL SOLUTION OF EQUATIONS GOVERNING LONGITUDINAL SUSPENSION-LINE WAVE MOTION DURING THE PARACHUTE UNFURLING PROCESS

By

Lamont Rozelle Poole

B.S.A.E., North Carolina State University

1970

A Thesis submitted to

The Faculty of

The School of Engineering and Applied Science

of The George Washington University in partial satisfaction

of the requirements for the degree of Master of Science

May 1973

Thesis directed by

John L. Whitesides, Jr.

Assistant Research Professor of Engineering

ACKNOWLEDGEMENTS

My deepest appreciation is extended to all those whose efforts contributed to this document. I am indebted to the National Aeronautics and Space Administration for allowing me the time and opportunity to conduct this study. Words of thanks are due to Dr. Earle K. Huckins, III, and Mr. Richard E. Turner for their technical advice, to Mr. Charles H. Whitlock and Mr. Andrew R. Wineman for their encouragement and administrative guidance, and particularly to Dr. John L. Whitesides, Jr., chairman of my advisory committee, for his advice in organizing the study and his suggestions in presenting the results.

ABSTRACT

Equations are presented which govern the dynamics of the lines-first parachute unfurling process, including wave motion in the parachute suspension lines. Techniques are developed for obtaining numerical solutions to the governing equations. Histories of tension at the vehicle obtained using the techniques are compared with flight test data, and generally good agreement is observed. Errors in computed results are attributed to several areas of uncertainty, the most significant being a poorly defined boundary condition on the wave motion at the vehicle-suspension line boundary.

TABLE OF CONTENTS

LIST OF TABLES

LIST OF FIGURES

LIST OF SYMBOLS

A	reference area, meters^2
C	damping coefficient of a single suspension line, newton-seconds
C_D	drag coefficient
F_{re}	unfurling resistance force, newtons
g	acceleration due to gravity, meters/second^2
h	altitude, meters
K'_{sec}	specific secant modulus of a single suspension line, newtons
ℓ	general spatial coordinate along unstressed suspension lines, measured from vehicle attachment point, meters
$\Delta\ell$	distance between adjacent spatial stations in numerical grid pattern, meters
ℓ_B	unfurled length (or, equivalently, spatial coordinate of parachute mass element exiting mouth of deployment bag), meters
L_p	total unstressed length of extended parachute, meters
L_{sl}	unstressed length of suspension lines, meters
m	mass, kilograms
m'	linear mass density of general parachute element exiting mouth of deployment bag, kilograms/meter
m'_{sl}	linear mass density of a single suspension line, kilograms/meter
n_{sl}	number of suspension lines
q_∞	freestream dynamic pressure, newtons/meter^2
t	time, seconds
t_{mf}	time from mortar fire, seconds

Δt	time increment between adjacent time stations in numerical grid pattern, seconds
u	unfurling rate or velocity at which parachute exits mouth of deployment bag, meters/second
v	velocity, meters/second
V_n	partial derivative with respect to time of deflection at juncture of suspension lines and canopy, meters/second
x	deployed distance of bag, measured rearward from base of vehicle, meters
y	general time-variant function
γ	flight-path angle, measured with respect to local horizontal, degrees
δ	displacement of any cross section of suspension lines from its unstressed position, meters
η	wake parameter

Subscripts:

b	deployment bag
B	deployment bag mouth
e	deployment bag plus its contents
i	ith time station (located at $t = i\Delta t$)
j	jth spatial station (located at $\ell = (j - 1)\Delta\ell$)
max	maximum
n	nth spatial station, which is located at juncture of suspension lines and canopy ($\ell = L_{sl}$)
sl	suspension line
v	vehicle
V	suspension-line attachment point at vehicle

1	first spatial station, which is located at suspension-line attachment point at vehicle ($\ell = 0$)

Dots over symbols denote time derivatives.

INTRODUCTION

The successful operation of a parachute depends not only on a proper inflation phase, during which large aerodynamic drag forces are generated by the inflating parachute, but also on a proper phase of deployment, during which the parachute suspension system and canopy are extended downstream of the towing vehicle to a stage at which the inflation phase can begin in a satisfactory manner. In a general configuration, the parachute suspension lines and canopy are folded and packed into a deployment bag which is stowed in the towing vehicle until desired trajectory conditions are reached. The bag is then deployed rearward from the vehicle, either by some forced-ejection device such as a mortar or by a small drogue or pilot parachute. As the bag travels rearward, the packed suspension system and, then, canopy are unfurled from the bag. A typical vehicle-parachute configuration during a lines-first deployment is shown in figure 1.

Interest in such decelerator systems for planetary entry vehicles has stimulated research in deployment dynamics which has resulted in significant improvements over earlier empirical methods (references 1 and 2). A primary need for simulating the deployment process is to determine the motion of the deployment bag relative to the towing vehicle. Knowledge of sequence of events and unfurling times, the rates at which parachute material is unfurled from the deployment bag, and the levels of tension generated in the suspension system during the process of unfurling are important from mission analysis and deployment system design standpoints.

Reference 3 presents an extensive discussion of deployment systems and methods for analyzing deployment dynamics. Though restricted to the case of an inextensible parachute, the techniques developed in reference 3 provide accurate simulation of vehicle trajectories and histories of deployment bag motion. The techniques also can be used to calculate reasonably accurate suspension-system tension histories, provided that averaged (as opposed to precise) parachute linear-mass-density profiles are employed.

The results presented in reference 4 indicate that suspension-line elasticity is an important parameter in the prediction of tension loads experienced during parachute inflation. The significance of elasticity during the lines-first deployment process is indicated by the analysis presented in reference 5. Through a steady-state solution to the linearized one-dimensional wave equation governing suspension-line elasticity, a technique was developed in reference 5 which provides quite accurate prediction of the snatch force generated as the parachute canopy begins to unfurl from the deployment bag. The consequences of neglecting wave mechanics in the modeling of suspension-line elasticity during the unfurling process were studied in reference 6. It was found that, by using a massless-spring-type model for the elasticity, quite accurate histories of vehicle and deployment bag motion could be calculated, as was the case using the inextensible model. Generally accurate histories of suspension-system tension could be calculated except during periods of rapid load fluctuation caused by abrupt changes in the linear mass density of successive

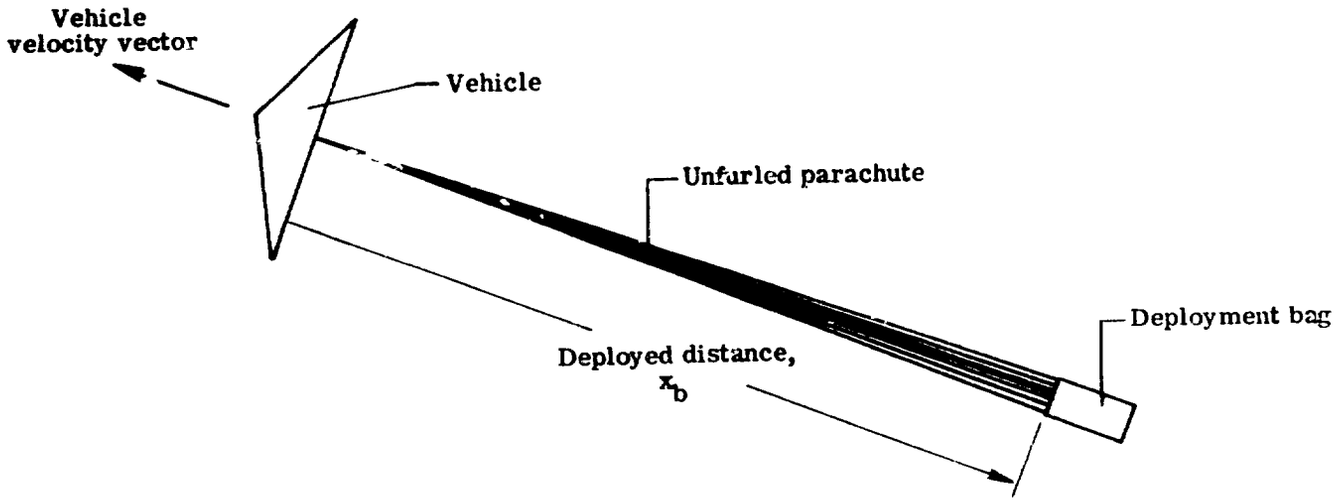

Figure 1.- Th[illegible]loyment configuration.

canopy mass elements unfurling from the deployment bag. Large fluctuations in material unfurling rate corresponding to these linear-mass-density changes were calculated, but the accuracy of these calculations was questioned due to the relative inaccuracy of the tension calculations. As a general conclusion, the inaccuracies were attributed to neglecting wave mechanics in the formulation of the model.

The present paper employs the equations developed in reference 6 for governing the two-body planar motion of a lines-first forced-ejection deployment in conjunction with the one-dimensional nonlinear wave equation governing suspension-line elast response. In light of the solution accuracy discussed in reference 6, the unfurling process is treated as two phases: a suspension-line unfurling phase, during which the formulation can be reduced to the massless-spring class; and a canopy unfurling phase, during which a solution to the complete set of equations must be obtained. Techniques are developed for obtaining a numerical solution to the governing equations. Generally good agreement between calculated results and flight test data is obtained by using the present model to simulate deployment loads and motions of two disk-gap-band parachute deployment flight tests.

ANALYSIS

In the analysis to follow, equations are presented which govern the dynamics of lines-first deployment of a parachute having elastic suspension lines. Equations are presented which govern the motion of the towing vehicle and the motion of the deployment bag relative to the vehicle. An expression relating the tension developed at the mouth of the deployment bag to the rate at which the parachute exits the mouth of the bag (the unfurling rate) is given. The equation and boundary conditions governing the longitudinal wave motion in the elastic suspension lines are developed. In addition, expressions are developed by which the elastic behavior of the suspension lines can be approximated by a massless-spring-class model during the phase of suspension-line unfurling.

For the purposes of this analysis, the vehicle and the deployment bag and its instantaneous contents are considered to be mass particles. The surface of the planet is considered to be flat, and surface-relative accelerations are considered to be inertial. The vehicle is assumed to be non-lifting, and its motion is restricted to a vertical plane. The motion of the deployment bag relative to the vehicle and the orientation of the tension vector in the parachute suspension lines are assumed to be parallel to the vehicle relative wind.

Equations of Motion

The forces affecting the motion of the vehicle and deployment bag are shown in Figure 2.

The motion of the vehicle is influenced by aerodynamic drag, tension in the parachute suspension system, and gravitational attraction. Under the previously mentioned assumptions, an expression was developed in reference 6 which governs the acceleration of the vehicle in the direction of its velocity vector, which is

$$\dot{v}_v = -\left[\frac{(C_D A)_v q_\infty + T_V}{m_v} + g \sin \gamma\right] \tag{1}$$

In addition, the following trajectory equations are required in order to specify fully the earth-relative planar motion of the vehicle

$$\dot{h} = v_v \sin \gamma \tag{2}$$

$$\dot{\gamma} = -\frac{g \cos \gamma}{v_v} \tag{3}$$

The motion of the deployment bag is influenced by aerodynamic drag, an unfurling resistance force, and gravitational attraction. An expression was developed, also in reference 6, which governs the acceleration of the deployment bag in the direction of the vehicle velocity vector, which is

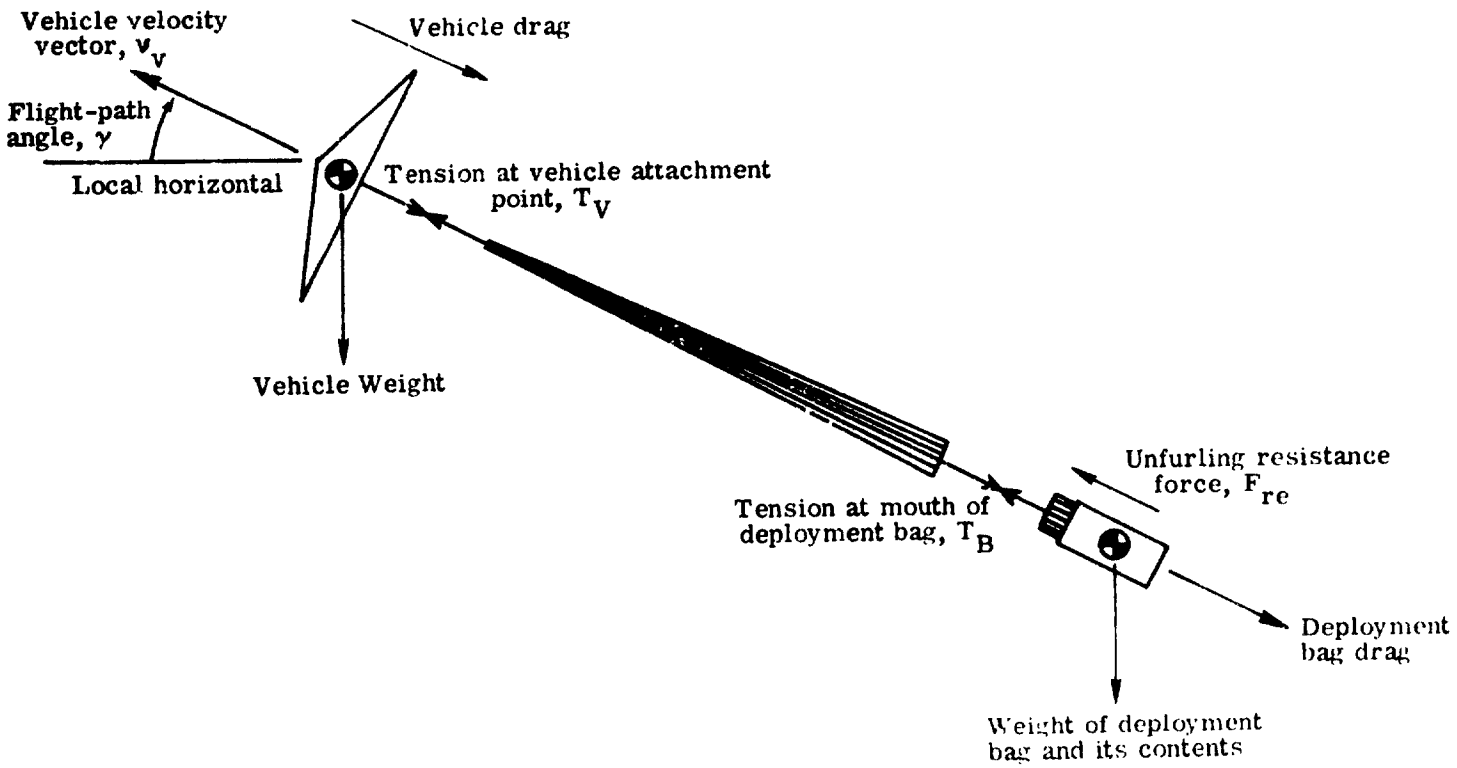

Figure 2.- Forces affecting motions of vehicle and deployment bag.

$$\dot{v}_b = -\left[\frac{\eta(C_D A)_b q_\infty - F_{re}}{m_e} + g \sin \gamma\right] \tag{4}$$

In this expression, the reduction in dynamic pressure acting on the bag due to the motion of the bag relative to the vehicle is also neglected. The velocity of the deployment bag relative to the vehicle can then be written, subsequent to solution of equations (1) and (4), as

$$\dot{x}_b = v_v - v_b \tag{5}$$

An additional expression relating the tension developed in the unfurling parachute at the mouth of the deployment bag to the linear mass density of the parachute element exiting the bag and the unfurling rate was given in reference 5, and can be written as

$$T_B = m'u^2 + F_{re} \tag{6}$$

The unfurling rate is, by definition, the rate of change of the spatial coordinate of the mouth of the deployment bag, or

$$u = \dot{\ell}_B \tag{7}$$

Suspension-System Elasticity

Complete definition of the motions of the deployment process requires the formulation of some relationship between the tension generated at the mouth of the deployment bag, the tension transmitted to the vehicle, the relative motion of the deployment bag, and the unfurling rate. Such a relationship is furnished by a mathematical model of the parachute elasticity. In the present paper, the parachute canopy is considered to be an inextensible structure due to its complex cloth-tape configuration, which is thought to undergo very little, if any, deformation during the unfurling process. The dynamic response of the suspension lines during the unfurling process can be determined most accurately by a mathematical model which considers the wave mechanics of the lines (reference 6). As the deployment motion is considered in the present paper to be one-dimensional, such a model requires only a single partial differential equation to govern the longitudinal wave motion in the lines.

The present model considers the parachute suspension system to consist of suspension lines only, which have negligible aerodynamic drag and uniform elastic and mass properties. The elastic state of the suspension lines can be represented by use of the coordinates and variables shown in Figure 3. The governing equation for the longitudinal motion of an arbitrary suspension-line element was developed in reference 6 and can be written, in light of the present assumptions, as

$$\frac{\partial^2 \delta}{\partial t^2} - \frac{1}{n_{sl} m'_{sl}} \frac{\partial T}{\partial \ell} = -\left[\frac{(C_D A)_v q_\infty + T_V}{m_v}\right] \qquad (8)$$

The elastic behavior of the element can be described by a relationship between the tension, T, and the displacement, δ, and its derivatives. Considering the tension to be a sum of static and dynamic components, this relationship can be written as

$$T = n_{sl}\left[K'_{sec} \frac{\partial \delta}{\partial \ell} + C \frac{\partial}{\partial t}\left(\frac{\partial \delta}{\partial \ell}\right)\right] \qquad (9)$$

The present model considers the specific secant modulus, K'_{sec}, to be a function of the strain, $\frac{\partial \delta}{\partial \ell}$, and assumes the damping coefficient, C, to be constant.

Boundary conditions at the point at which the suspension lines attach to the vehicle and at the mouth of the deployment bag (or at the juncture of the suspension lines and the canopy, for times after which the lines have been completely unfurled) must also be prescribed. The present paper considers the suspension lines to be attached to the vehicle in a manner such that no deflection in the lines is allowed at that point. Mathematically, this condition can be stated as

$$\delta|_{\ell = 0} = 0 \qquad (10)$$

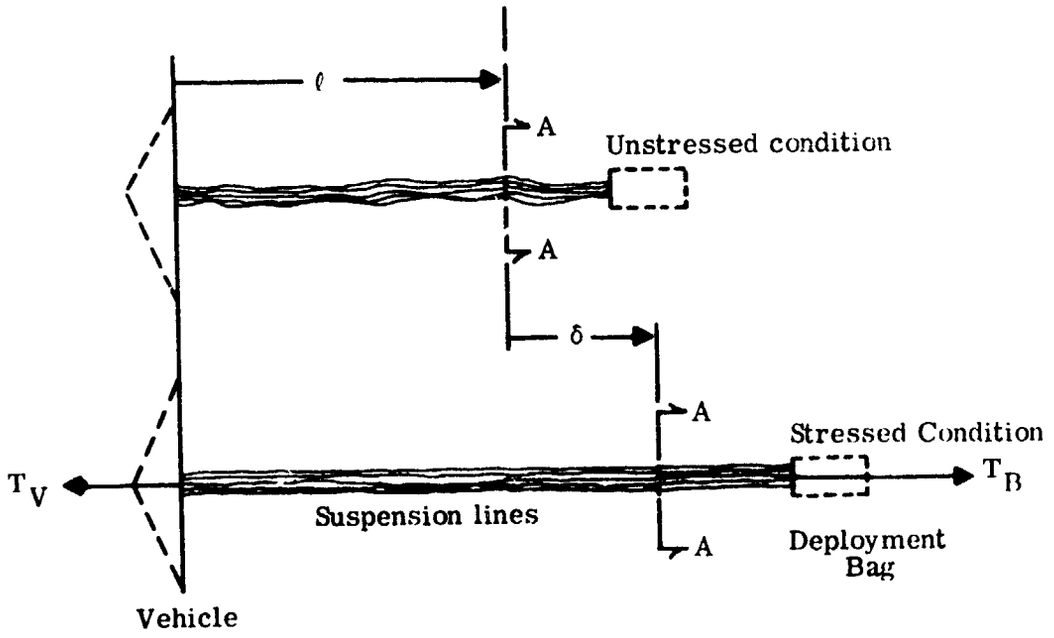

Figure 3.- Coordinates defining suspension-line geometry.

The tension is subject to the boundery condition at the mouth of the deployment bag which is given in equation (6). Additionally, an equation of compatability between the motion of the deployment bag and the motion of the exiting parachute element can be written as

$$\left.\frac{D\delta}{Dt}\right|_{\ell=\ell_B} = \dot{x}_b - u, \quad (0 \leq \ell_B \leq L_{sl}) \tag{11}$$

Suspension-Line Unfurling Phase

It was concluded in reference 6 that a massless-spring-type model of the suspension-line elasticity provides acceptable simulation of deployment loads and motions during periods of small load fluctuations, as is the case during the suspension-line unfurling phase. In order to avoid the numerical complexities of solving a partial differential equation in an expanding space, a similar model is employed in the present analysis to govern the suspension-line unfurling phase. Under the assumption of a massless-spring model, equation (8) reduces to

$$\frac{\partial T}{\partial \ell} = 0 \quad , \quad (0 \leq \ell_B \leq L_{sl}) \tag{12}$$

Therefore the tension is constant throughout the lines at any particular time, or

$$T_V = T_B \quad , \quad (0 \leq \ell_B \leq L_{sl}) \tag{13}$$

The total derivative in equation (11) can be expanded into local and convective terms and, considering the definition of the unfurling rate as given by equation (7), can be written as

$$\left.\frac{D\delta}{Dt}\right|_{\ell=\ell_B} = \left.\frac{\partial\delta}{\partial t}\right|_{\ell=\ell_B} + u \left.\frac{\partial\delta}{\partial\ell}\right|_{\ell=\ell_B} \tag{14}$$

Since the strain rates experienced during suspension-line unfurling are very small, the dynamic component of the tension expressed by equation (9) can be neglected. Then equation (9) can be solved for the strain $\frac{\partial\delta}{\partial\ell}$, which can be evaluated at $\ell=\ell_B$ and substituted into equation (14), resulting in

$$\frac{D\delta}{Dt} = \left.\frac{\partial\delta}{\partial t}\right|_{\ell=\ell_B} + u \frac{T_B}{n_{sl} K'_{sec}} \tag{15}$$

T_B can be replaced in equation (15) by its definition as given in equation (6) and the entire expression substituted into equation (11). This results in a cubic expression for the equilibrium unfurling rate at any time, which is

$$u^3 + \frac{K'_{sec}}{m'_{sl}}\left(1 + \frac{F_{re}}{n_{sl} K'_{sec}}\right) u - \frac{K'_{sec}}{m'_{sl}} \left(\dot{x}_b - \left.\frac{\partial\delta}{\partial t}\right|_{\ell=\ell_B}\right) = 0 \tag{16}$$

However the deflection rate at the bag mouth, $\left.\frac{\partial\delta}{\partial t}\right|_{\ell=\ell_B}$, is several orders of magnitude smaller than the relative bag velocity during the suspension-line unfurling phase. Thus, equation (16) can be reduced to

$$u^3 + \frac{K'_{sec}}{m'_{sl}}\left(1 + \frac{F_{re}}{n_{sl}\,K'_{sec}}\right)u - \frac{K'_{sec}}{m'_{sl}}\,\dot{x}_b = 0 \qquad (17)$$

Equations (1) through (7), in conjunction with equations (13) and (17), thus govern the suspension-line unfurling phase.

Canopy Unfurling Phase

The canopy unfurling phase begins when the suspension lines are completely unfurled from the bag. As rapid load fluctuations characteristically occur during this phase, a solution to the equation governing wave motion in the suspension lines must be obtained (equation (8)). Initial conditions on the motion of the suspension lines at the beginning of this phase are prescribed by the massless-spring-type solution obtained during the previous phase. As the tension (and thus strain) at any particular time is uniform throughout the length of the lines in that solution, the initial displacement profile must be linear (with $\delta|_{\ell=0} = 0$) in order to assure compatability between the phases. The initial displacement rate profile is assumed to be identically zero, in accordance with the assumption in effect during the previous phase. During the canopy unfurling phase, the boundary condition expressed by equation (11) is applied at the spatial coordinate of the juncture of the suspension lines and canopy, which is stationary. Thus, the boundary condition can be reduced to partial derivative form and can be expressed as

$$\left.\frac{\partial \delta}{\partial t}\right|_{\ell=L_{sl}} = \dot{x}_b - u, \quad (L_{sl} < \ell_B \leq L_p) \tag{18}$$

A simultaneous solution of equations (1) through (9), in conjunction with the boundary conditions given in equations (10) and (18) and the initial conditions described previously, defines the loads and motions of the canopy unfurling phase.

TECHNIQUES FOR NUMERICAL SOLUTION OF GOVERNING EQUATIONS

In order to define the loads and motions of both the suspension-line and canopy unfurling phases, a solution to the ordinary differential equations governing the motion of the vehicle and deployment bag must be obtained. During the canopy unfurling phase, a solution to the partial differential equation governing wave motion in the suspension lines, subject to prescribed initial and boundary conditions, must also be obtained. Techniques for obtaining proper solutions during both unfurling phases have been developed using standard finite-difference methods, such as those described in reference 7, and are described in this section.

Suspension-Line Unfurling Phase

The suspension-line unfurling phase is governed by six first-order ordinary differential equations (equations (1) through (5) and (7)) in conjunction with an algebraic equation for calculating the unfurling rate (equation (17)) and two expressions for calculating the tension generated at the mouth of the deployment bag and the tension transmitted to the vehicle (equations (6) and (13)). Initial values of the variables (v_v, h, γ, v_b, x_b, and ℓ_B) of course depend on flight trajectory conditions and the individual system configuration. The set of differential equations is integrated using the single-step forward-difference technique suggested by Euler. Given the value of the first derivative of a time-variant function y at time station i, Euler's technique is used to calculate y at time station i+1 as follows:

$$y_{i+1} = y_i + \Delta t[\dot{y}_i] \tag{19}$$

This procedure is quite simple and is particularly useful for integrating smooth functions such as those derivatives of interest during this phase. Since the frictional resistance force F_{re} and the suspension-line linear mass density m'_{sl} are constants and the specific secant modulus K'_{sec} is a smoothly varying function of the strain (and, actually, is nearly constant during this phase) equations (17) and (6) can be solved without iteration for the unfurling rate and tension at the deployment bag mouth, respectively.

Canopy Unfurling Phase

The motions of the vehicle and deployment bag during the canopy unfurling phase are again governed by the six first-order ordinary differential equations as described in the previous section. Values of the variables of concern at the initiation of this phase are, of course, their values at the end of the suspension-line unfurling phase. These differential equations are again integrated using Euler's technique.

A solution must be obtained simultaneously to the second-order partial differential equation governing wave motion in the suspension lines (equation (8)) in conjunction with the elastic model expressed by equation (9). The wave equation is subject to the boundary condition of no deflection at the vehicle attachment point, as expressed by equation (10), and to the boundary condition of compatability at the

juncture of the suspension lines and canopy, as expressed by equation (18). Initial conditions on the wave motion are those discussed in the analysis section, namely, the initial strain profile is linear, with $\delta|_{\ell=0} = 0$, and the initial deflection rate profile is identically zero. The wave equation can be solved by using standard central-difference formulations which can be derived using the grid pattern and subscripts shown in Figure 4.

The derivative $\frac{\partial^2\delta}{\partial t^2}$ at any interior point can be approximated by the following central-difference equation:

$$\left.\frac{\partial^2\delta}{\partial t^2}\right|_{i,j} = \frac{\delta_{i+1,j} - 2\delta_{i,j} + \delta_{i-1,j}}{(\Delta t)^2} \tag{20}$$

The tension gradient $\frac{\partial T}{\partial \ell}$ at any interior point can be approximated by a central difference equation by using the half-station concept, as follows:

$$\left.\frac{\partial T}{\partial \ell}\right|_{i,j} = \frac{T_{i,j+1/2} - T_{i,j-1/2}}{\Delta \ell} \tag{21}$$

The tensions at the half stations $i,j+1/2$ and $i,j-1/2$ are a function of the local strain and strain rate, as expressed by equation (9). The strain at stations $i,j+1/2$ and $i,j-1/2$ can be evaluated by using the following difference approximations:

$$\left.\frac{\partial \delta}{\partial \ell}\right|_{i,j+1/2} = \frac{\delta_{i,j+1} - \delta_{i,j}}{\Delta \ell} \tag{22}$$

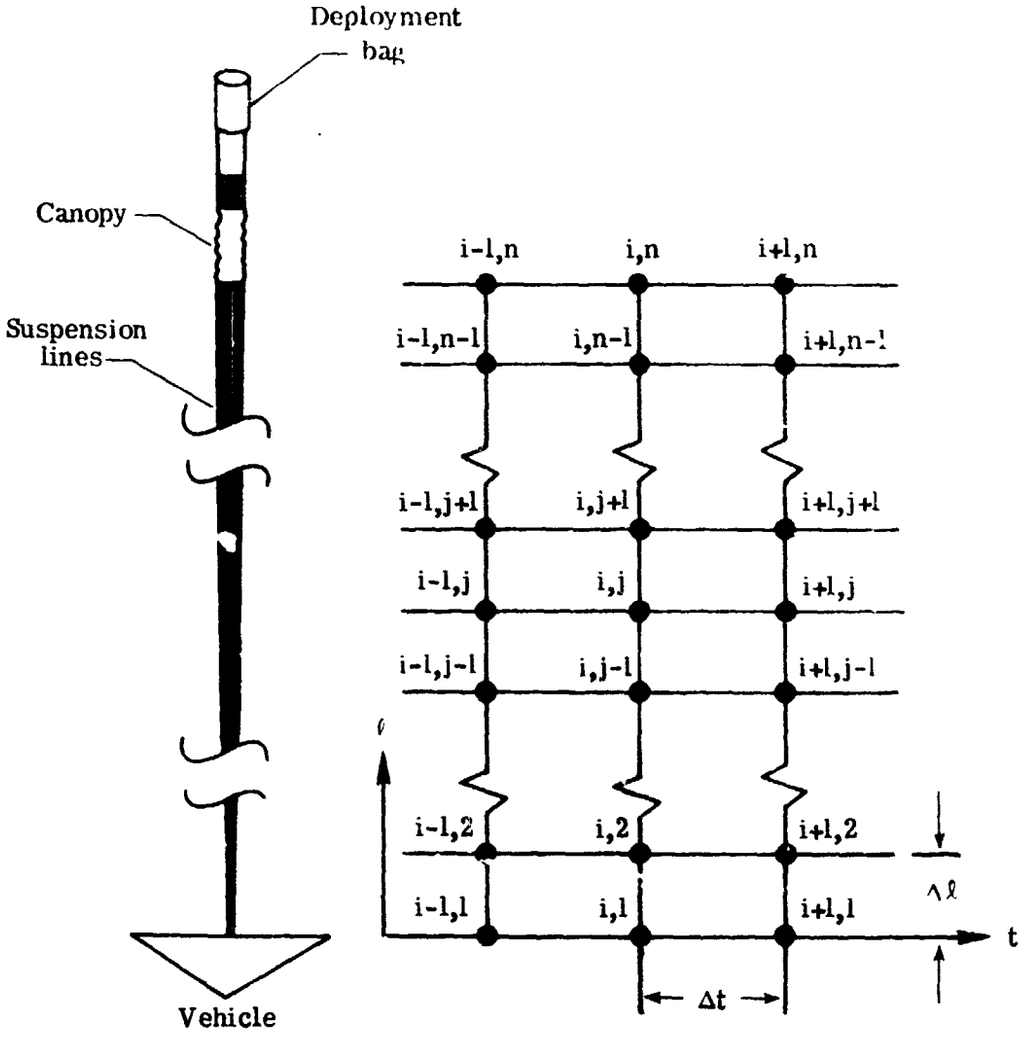

Figure 4.- Grid pattern for finite-difference approximations.

$$\left.\frac{\partial \delta}{\partial \ell}\right|_{i,j-1/2} = \frac{\delta_{i,j} - \delta_{i,j-1}}{\Delta \ell} \tag{23}$$

The strain rates at these two stations can be evaluated by using the following difference approximations in conjunction with equations (22) and (23).

$$\frac{\partial}{\partial t}\left(\frac{\partial \delta}{\partial \ell}\right)\Big|_{i,j+1/2} = \frac{\left.\frac{\partial \delta}{\partial \ell}\right|_{i,j+1/2} - \left.\frac{\partial \delta}{\partial \ell}\right|_{i-1,j+1/2}}{\Delta t} \tag{24}$$

$$\frac{\partial}{\partial t}\left(\frac{\partial \delta}{\partial \ell}\right)\Big|_{i,j-1/2} = \frac{\left.\frac{\partial \delta}{\partial \ell}\right|_{i,j-1/2} - \left.\frac{\partial \delta}{\partial \ell}\right|_{i-1,j-1/2}}{\Delta t} \tag{25}$$

A value of the specific secant modulus at each of the half-stations can be found explicitly as a function of the local strain. Then values of local strain, strain rate, and specific secant modulus can be used in equation (9) to calculate the tension at the half-stations. Thus, the approximations given by equations (20) and (21) can be substituted into equation (8), resulting in a difference approximation to the wave equation which can be used for calculating future values of the deflection δ at station j. This approximation is

$$\delta_{i+1,j} = 2\delta_{i,j} - \delta_{i-1,j} + (\Delta t)^2 \left\{ -\left[\frac{(C_D A)_v q_\infty + T_v}{m_v}\right] + \frac{1}{n_{s1} m'_{s1}} \left[\frac{T_{i,j+1/2} - T_{i,j-1/2}}{\Delta \ell}\right] \right\} \tag{26}$$

In using the difference approximation given by equation (26), care must be taken in the selection of values of Δt and $\Delta \ell$ in order to assure a stable solution. Stability can be assured if the ratio of $\Delta \ell$ to Δt is greater than the maximum wave propagation velocity anticipated in the course of the solution. Using the classical definition of wave velocity, the stability criterion which must be satisfied can be stated as

$$\frac{\Delta \ell}{\Delta t} \geq \left(\frac{K'_{sec,max}}{m'_{sl}} \right)^{1/2} \tag{27}$$

where $K'_{sec,max}$ is the maximum value of the specific secant modulus in the range of suspension-line strains expected in the course of the solution.

The deflection at spatial station n, which is located at the juncture of the suspension lines and canopy ($\ell = L_{sl}$), must be obtained through a simultaneous solution to the wave equation (equation (8)) and the boundary condition of compatability expressed by equation (18). In the development of a technique for obtaining this solution, it is assumed that the tension level is constant at all points throughout the canopy (acceleration of the unfurled portion of the canopy is neglected). Then the tension at the juncture of the suspension lines and canopy equals the tension being generated at the mouth of the deployment bag, which is expressed by equation (6). It is also assumed that the linear-mass-density profile of the canopy can be represented mathematically in a manner such that no discontinuities are present.

The inter-relationship of equations (6), (8), and (18) suggests some type of iterative solution technique. Such a technique can be developed by first treating the wave equation, equation (8), as two first-order equations. By defining

$$V_n = \frac{\partial \delta}{\partial t}\Big|_{\ell=L_{sl}} \tag{28}$$

equation (8) can be written as

$$\frac{\partial V_n}{\partial t} = \frac{1}{n_{sl} m'_{sl}} \frac{\partial T}{\partial \ell}\Big|_{\ell=L_{sl}} - \left[\frac{(C_D A)_v q_\infty + T_V}{m_v}\right] \tag{29}$$

The tension gradient in equation (29) can be approximated by the following backward-difference equation (again using the subscripts shown in Figure 4):

$$\frac{\partial T}{\partial \ell}\Big|_{i,n} = \frac{T_B|_i - T_{i,n-1/2}}{\frac{1}{2}\Delta\ell} \tag{30}$$

In this equation, T_B is prescribed by equation (6), and $T_{i,n-1/2}$ can be calculated using the difference procedures outlined previously. A first estimate of the integral of equation (29) can then be calculated using Euler's method as given by equation (19), or

$$V_n|_{i+1} = V_n|_i + \Delta t \left[\frac{\partial V_n}{\partial t}\Big|_i\right] \tag{31}$$

Provided that an estimate of $\dot{x}_b$ at time station i+1 is known, a first estimate of the unfurling rate at that time station can be calculated using equation (18), or

$$u_{i+1} = \dot{x}_b\Big|_{i+1} - V_n\Big|_{i+1} \tag{32}$$

This value for the unfurling rate is used in equation (6) to calculate a first estimate of the tension at the bag mouth (and, thus, at spatial station n) at time station i+1. However, since the linear mass density of successively unfurling elements can be varying quite rapidly, this value of the tension at the bag can be substantially different from the value at the previous time station. Therefore, it is necessary to iterate on the solution. Ideally, the iteration procedure should include solution of equation (26) (at all spatial stations other than station n) and integration of equation (28), in order to update the array of deflection values δ for a updated estimate of the tension at station n - 1. In consideration of the fact that such a series of calculations would require extensive computer time, and also that, for sufficiently small time steps, changes in the deflection array will be small in comparison to changes in V_n, the deflection array is not updated until the iteration on the boundary solution has converged.

In light of these considerations, the iteration procedure is structured as follows:

(1) The first estimate of $T_B|_{i+1}$, which has been calculated previously, is substituted back into equation (30) and an estimate of the tension gradient at time station $i+1$ is calculated as follows:

$$\frac{\partial T}{\partial \ell}\Big|_{i+1,n} = \frac{T_B|_{i+1} - T_{i,n-1/2}}{\frac{1}{2}\Delta\ell} \tag{33}$$

(2) This value of the tension gradient can be substituted into equation (29) and a value for $\frac{\partial V_n}{\partial t}\Big|_{i+1}$ can be calculated. If this new value $\frac{\partial V_n}{\partial t}\Big|_{i+1}$ is within some error bound of the previous value $\frac{\partial V_n}{\partial t}\Big|_{i}$, the iteration procedure has converged.

(3) If the error criterion is not satisfied, a new estimate of the integral of equation (28) can be obtained using the trapezoidal method of numerical integration, which can be written as

$$V_n|_{i+1} = V_n|_i + \frac{\Delta t}{2}\left[\frac{\partial V_n}{\partial t}\Big|_i + \frac{\partial V_n}{\partial t}\Big|_{i+1}\right] \tag{34}$$

This new estimate of $V_n|_{i+1}$ can then be substituted into equation (32) to calculate a second estimate of the unfurling rate u_{i+1}. A second estimate of $T_B|_{i+1}$ can then be calculated, again using equation (6). The procedure is then repeated until two successive values of $\frac{\partial V_n}{\partial t}\Big|_{i+1}$ lie within the error bound of each other.

Since a converged value of $V_n|_{i+1}$ has also been found, it can be used in a trapezoidal integration scheme to find $\delta_{i+1,n}$, as follows:

$$\delta_{i+1,n} = \delta_{i,n} + \frac{\Delta t}{2}\left[V_n|_i + V_n|_{i+1}\right] \tag{35}$$

The final parameter to be evaluated is the tension at the point at which the suspension lines attach to the vehicle, T_V. The deflection δ at this point is assumed to be equal to zero, as expressed by equation (10). The basic partial differential equation (equation (8)) also holds at this point. By combining these two equations, an expression for calculating the tension gradient at the vehicle attachment point can be derived.

Since the deflection at the attachment point is always zero, its derivatives with respect to time, namely $\frac{\partial^2 \delta}{\partial t^2}\Big|_{\ell=0}$, are also zero. Thus, for this point, equation (8) can be reduced to

$$\frac{\partial T}{\partial \ell}\Big|_{\ell=0} = n_{sl} m'_{sl} \left[\frac{(C_D A)_v q_\infty + T_V}{m_v} \right] \tag{36}$$

An additional expression for this tension gradient can be found by expanding the tension at the mid-point of the grid space between spatial stations 1 and 2 (station 3/2) into a Taylor's Series about station 1 (at which $\ell = 0$). Neglecting second- and higher-order terms, this expansion is

$$T_{i,3/2} = T_{i,1} + \frac{\Delta \ell}{2} \frac{\partial T}{\partial \ell}\Big|_{i,1} \tag{37}$$

The tension at station i, 3/2 can be calculated numerically by using the difference procedures outlined previously, with the subscript $j = 1$. Since the tension gradient in equation (37) can be evaluated directly by using equation (36), the tension at the attachment point,

$T_{i,1}$, can then be evaluated directly as

$$T_{i,1} = T_{i,3/2} - \frac{\Delta\ell}{2} n_{sl} m'_{sl} \left[\frac{(C_D A)_v q_\infty + T_V}{m_v} \right] \qquad (38)$$

Ideally, since T_V (which, numerically, is also $T_{i-1,1}$) appears on the right-hand side of equation (38), a scheme for iterating on this equation in some manner until T_V and $T_{i,1}$ converge to the same value would be preferred. However, since m'_{sl} is generally an extremely small number, appreciable changes in T_V result in only minute changes in the magnitude of the tension gradient (equation (36)), and thus would alte. only slightly the value of $T_{i,1}$ in successive iterations. Thus, equation (38) is solved only once at each time step in the present paper.

The sequence of numerical calculations described in this section is outlined in Figure 5.

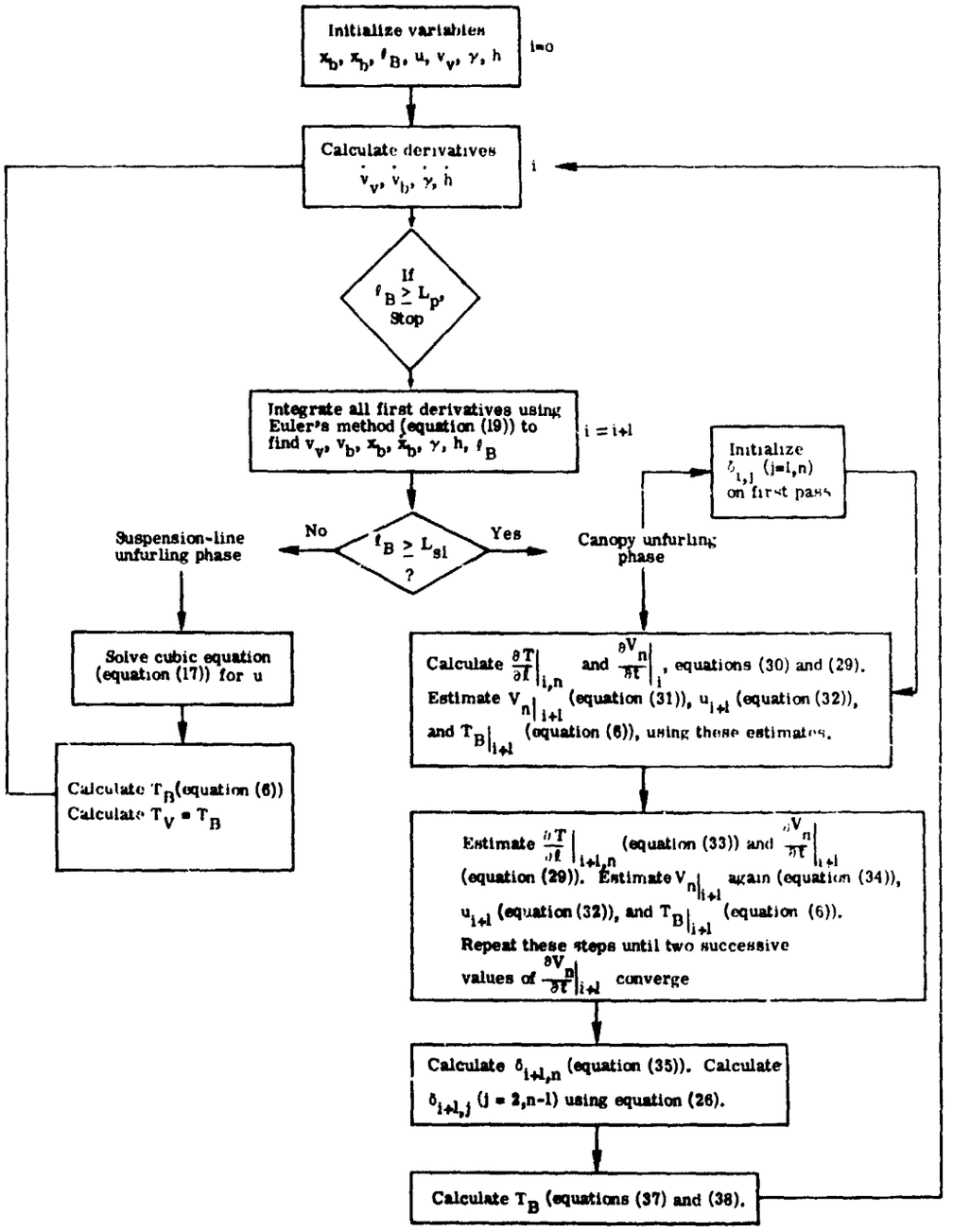

Figure 5.- Sequence of numerical procedures.

RESULTS AND DISCUSSION

A precise treatment of suspension-line wave motion during the parachute unfurling process is virtually impossible due to non-uniform mass and elastic characteristics, multi-dimensional motion, and poorly defined boundary conditions to which the motion is subject. The present method combines the planar representation of vehicle and bag motions with an idealized treatment of the wave motion in an effort to achieve reasonably accurate simulation of motions and loads. In order to evaluate the accuracy of the present method, it was used to calculate deployment loads and motions for two flight tests of disk-gap-band parachutes: the second balloon-launched flight test of the NASA Planetary Entry Parachute Program, B/L-2 (reference 8) and the flight test of vehicle AV-4 of the NASA Balloon Launched Decelerator Test Program (reference 9). Physical system data and parachute mass distributions for the two flight tests are presented and discussed in the appendix. As there is an absence of data, a numerical value for the suspension-line damping coefficient was determined parametrically. As the suspension system never became slack during the two flight test deployments the damping coefficient selected was the smallest value required to numerically maintain tension at the vehicle attachment point during the unfurling process.

Computed histories of unfurled length for the two flight tests are shown in Figure 6 and compared with test data points corresponding to mortar fire, line stretch, and estimated bag strip. The computed

histories exhibit very good agreement with flight test data.

A sequence of computed profiles of tension in the parachute suspension lines is presented for the B/L-2 flight test in Figures 7, 8, and 9. Figure 7a shows the state of the suspension lines just prior to the emergence of the skirt of the parachute canopy from the bag. The tension is constant along the length of the lines as is consistent with the assumptions made in the solution during the suspension-line unfurling phase. Unfurling of the lower edge of the band from the bag generates a sharp peak in the tension profile, as is shown in Figure 7b. As this peak travels down the suspension lines, it is damped and spread; Figure 7c shows the wave as it strikes the vehicle. The reflected wave is shown traveling back up the suspension lines in Figure 8a. The unfurling of the top of the band section of the canopy from the bag generates a second peak in the tension profile, which is shown in Figure 8b. This wave again is damped and spread as it travels toward the vehicle; the tension profile as the second wave strikes the vehicle is shown in Figure 8c. Unfurling of the bottom edge of the disk section of the canopy from the bag generates a third wave, which is shown departing the juncture of the suspension lines and canopy in Figure 9a. Figure 9b shows the third wave striking the vehicle as the reflected second wave reaches the juncture. Although interaction of generated and reflected waves causes some fluctuation in the tension at the vehicle attachment point after the third wave has reflected, the tension at that point decays rather smoothly due to the decreased tension being generated at

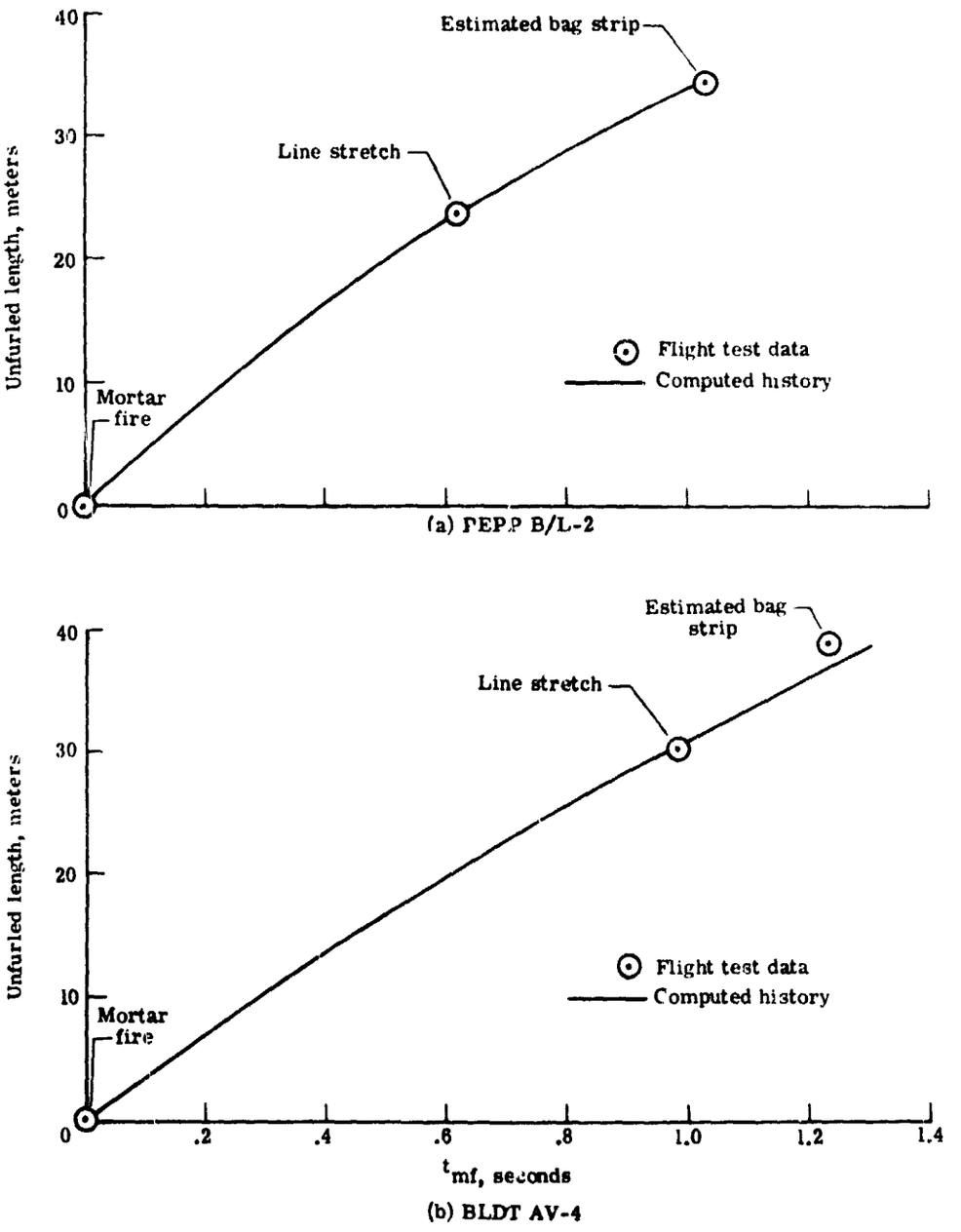

Figure 6.- Comparison of computed histories of unfurled length with flight test data.

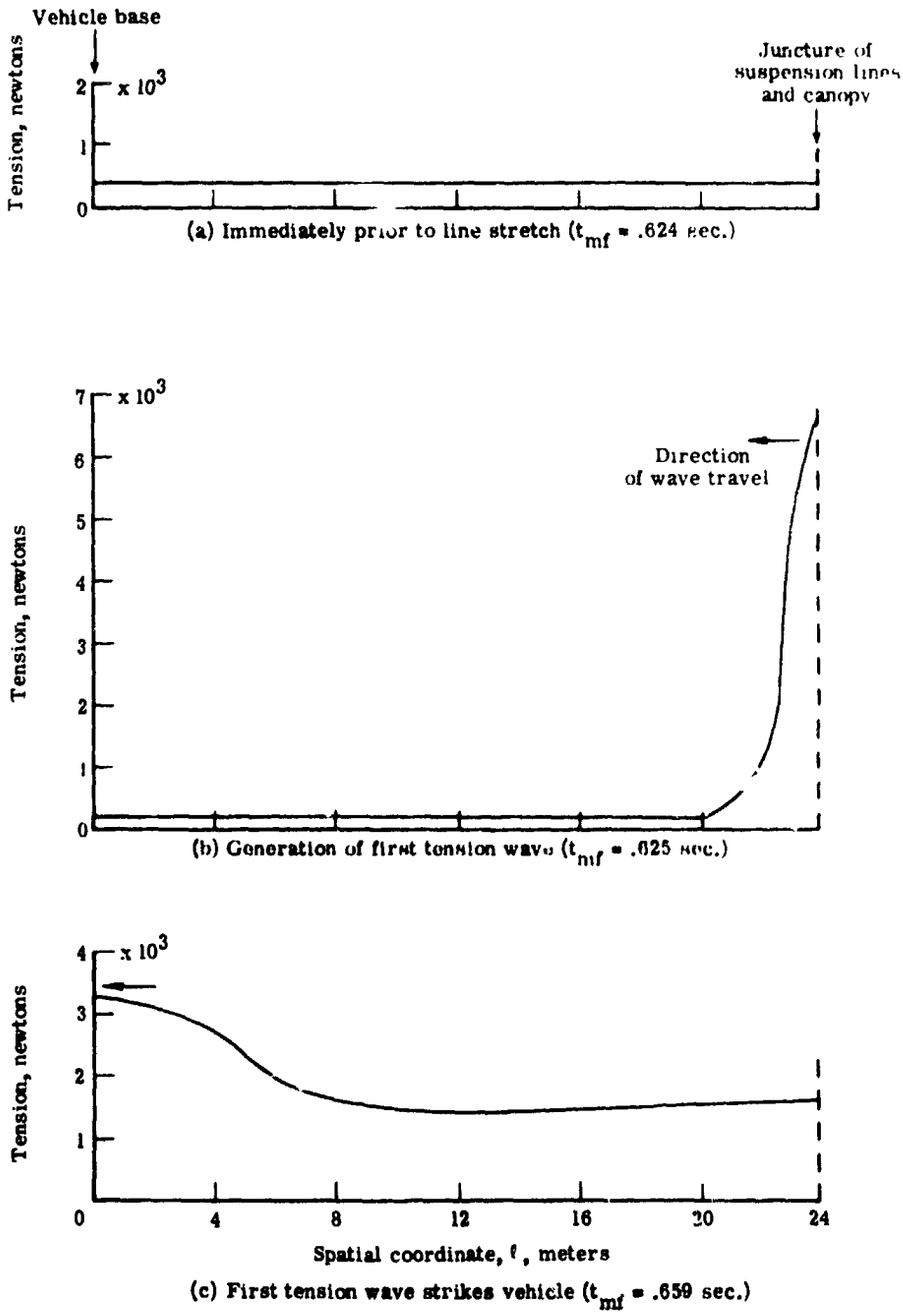

Figure 7.- Computed profiles of tension in suspension lines during PEPP B/L-2 parachute deployment.

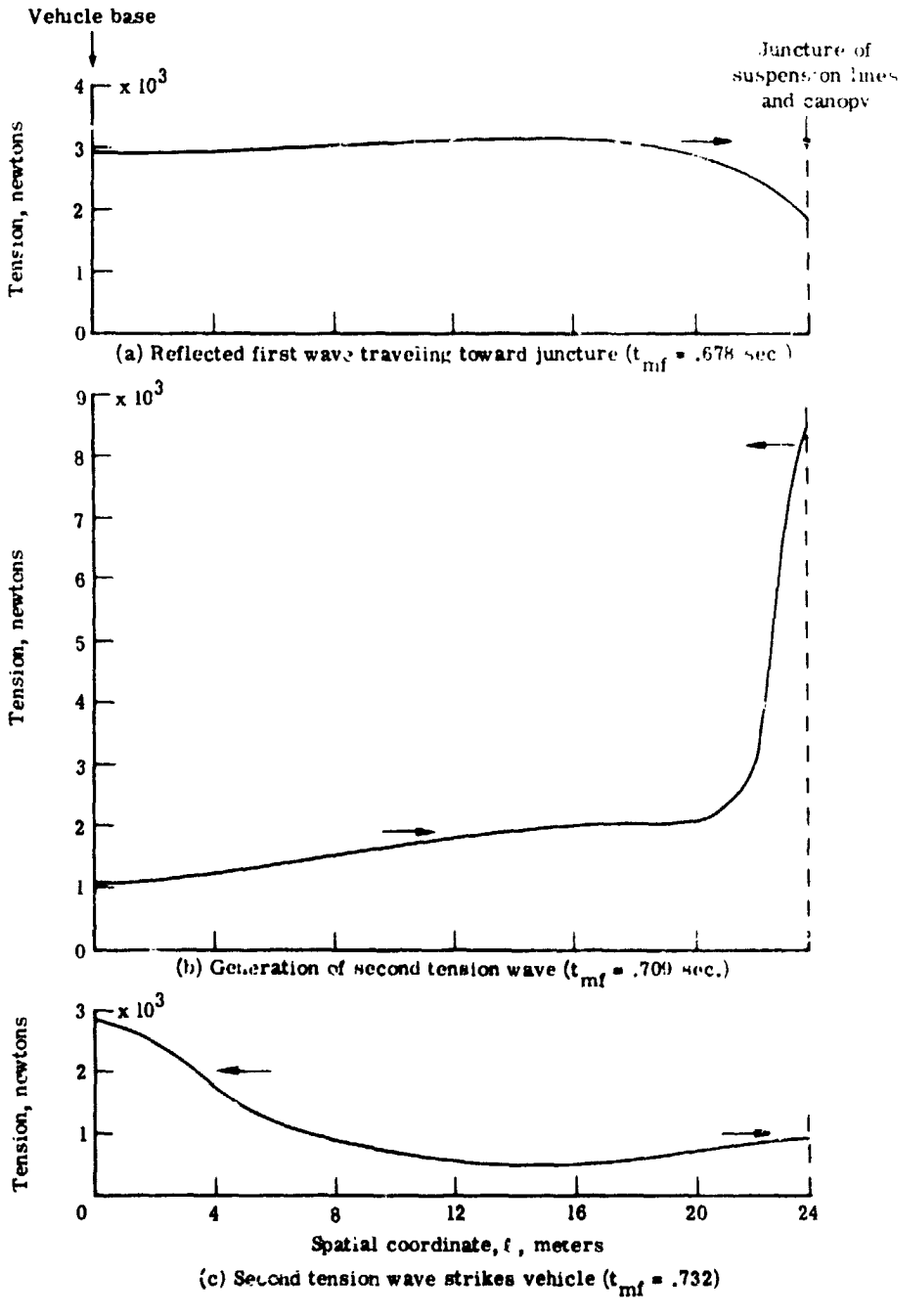

Figure 8.- Computed profiles of tension in suspension lines during PEPP B/L-2 parachute deployment (t_{mf} = .678, .709, and .732 sec).

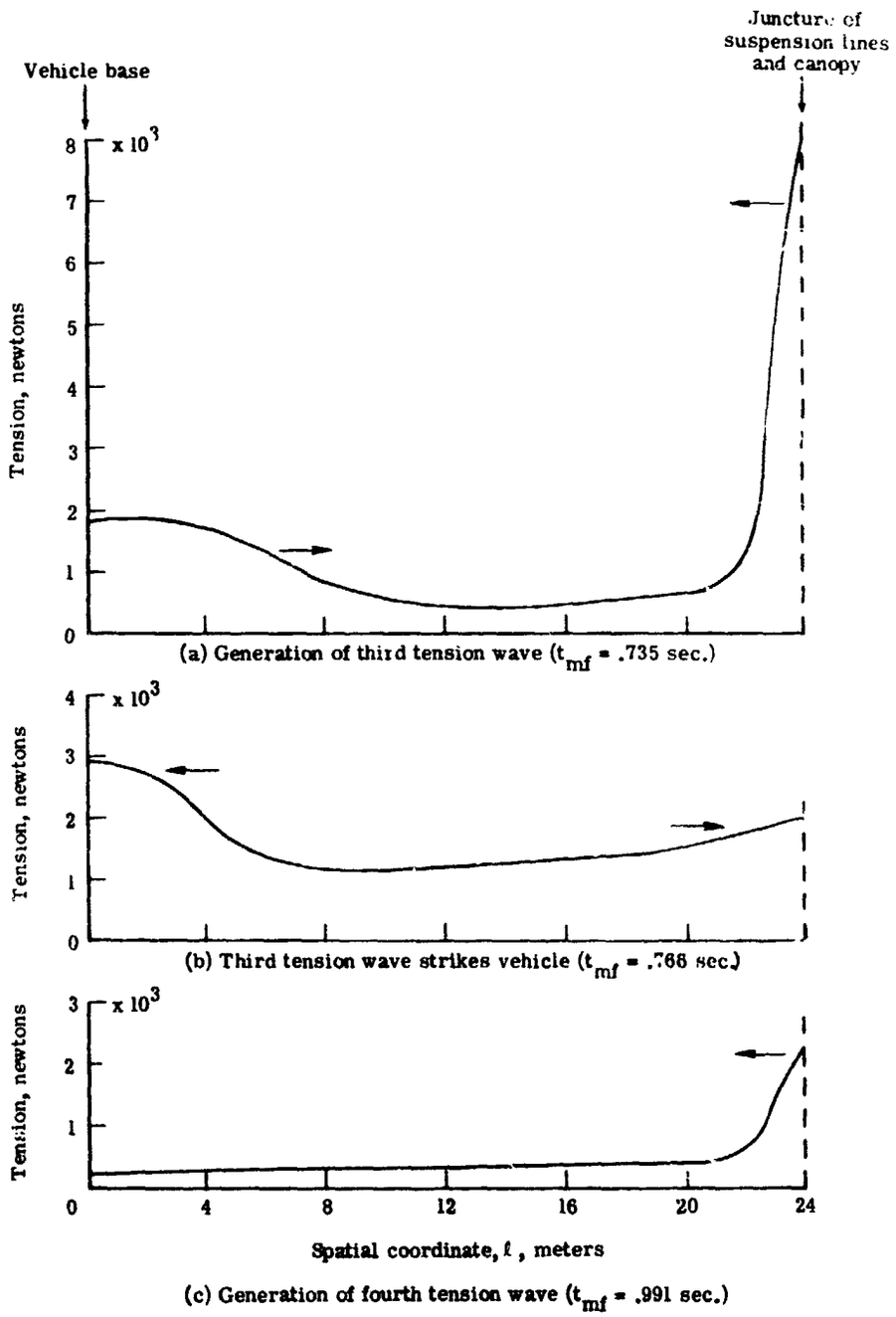

Figure 9.- Computed profiles of tension in suspension lines during PEPP B/L-2 parachute deployment (t_{mf} = .735, .766, and .991 sec).

the bag mouth as the disk unfurls. A fourth wave (of smaller magnitude) is generated upon the unfurling of the vent edge from the bag as is shown in the profile in Figure 9c. However, bag strip occurs before this fourth wave reaches the vehicle.

Tension profiles very similar in nature to those shown in Figures 7, 8, and 9 were obtained in the simulation of the AV-4 flight test. In the interest of brevity, only three of these are shown. Figure 10a shows the wave which is generated by the unfurling of the lower edge of the band as it leaves the juncture of the suspension lines and canopy. Figure 10b shows the second wave, which is generated by the unfurling of the top edge of the band, as it leaves the juncture and also shows the damped, reflected first wave traveling back toward the juncture. The profile shown in Figure 10c shows the third wave, which is generated by the unfurling of the lower edge of the disk, leaving the juncture as the second wave is approaching the vehicle.

Histories of the computed tension at the vehicle attachment point are compared with flight test data histories in Figure 11, for B/L-2, and in Figure 12, for AV-4. Peak loads shown in the initial half of each flight test history are attributed to phenomena which are not associated with the dynamics of unfurling and, as such, are not included in the present mathematical model. There is very good agreement in occurrence times of peak loads between the flight-test-data histories and the histories computed using the present method. Although agreement in peak load magnitudes is only fair, the results computed using the present method show considerable improvement over

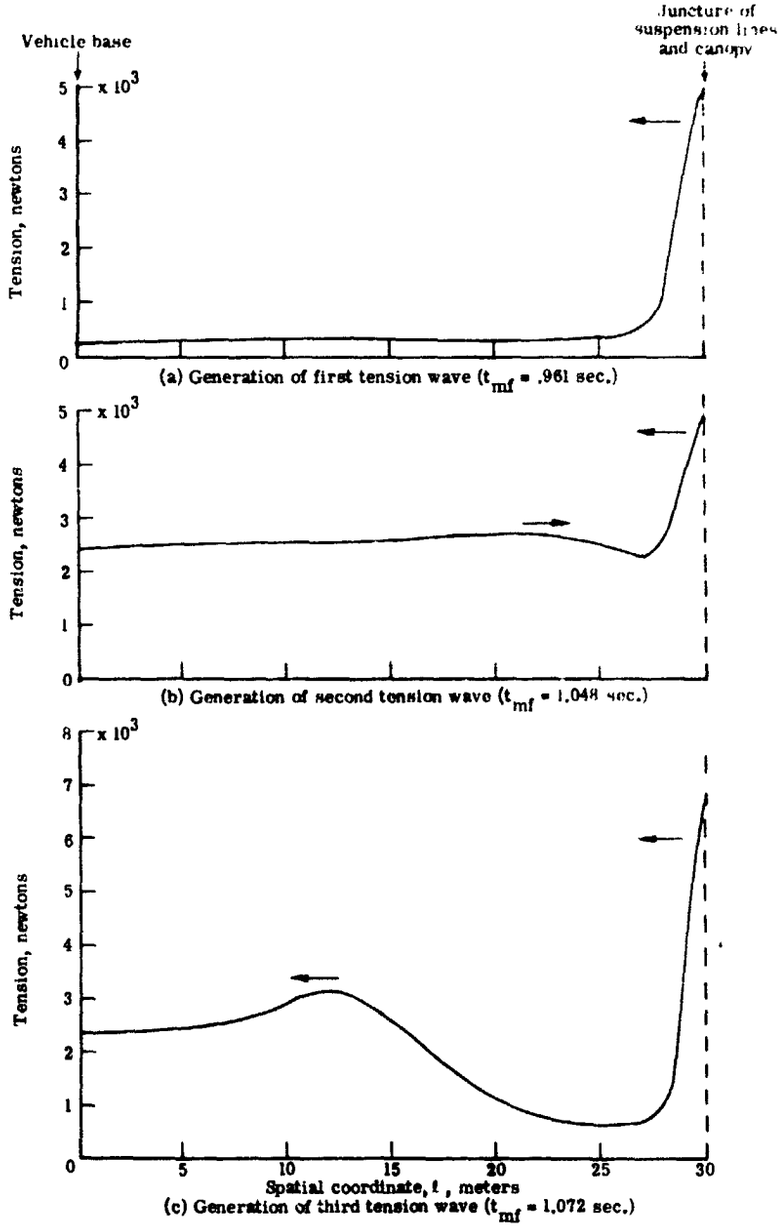

Figure 10.- Computed profiles of tension in suspension lines during BLDT AV-4 parachute deployment.

the results obtained using the massless-spring model (reference 6). Errors in the present computed histories can be attributed to several areas of uncertainty:

(1) Lack of data concerning the elastic response of suspension-line material at very high loading frequencies.

(2) Probable damping of waves generated by the unfurling of upper sections of the canopy as they are propagated through sections of the canopy which have been unfurled previously.

(3) Dispersions of wave propagation velocities between individual suspension lines.

(4) A poorly-defined boundary condition at the vehicle boundary. In flight tests, the suspension-lines are, in general, attached to a multi-legged, webbed bridle system, which in turn is attached in some manner to the vehicle itself. The bridle webbing probably exhibits rather severe damping effects and, in addition, waves reaching the vehicle itself are probably partially absorbed rather than totally reflected.

Computed histories of relative deployment bag velocity and unfurling rate for the two flight tests are presented in Figure 13. Similar trends are exhibited in both flights. The relative bag velocity decays smoothly due to deceleration of the towing vehicle. The general trend of the unfurling rate is a similar decay. However, sharp decreases in the unfurling rate occur when sudden increases in the linear mass density of the unfurling parachute are encountered; conversely, when sudden decreases in the linear

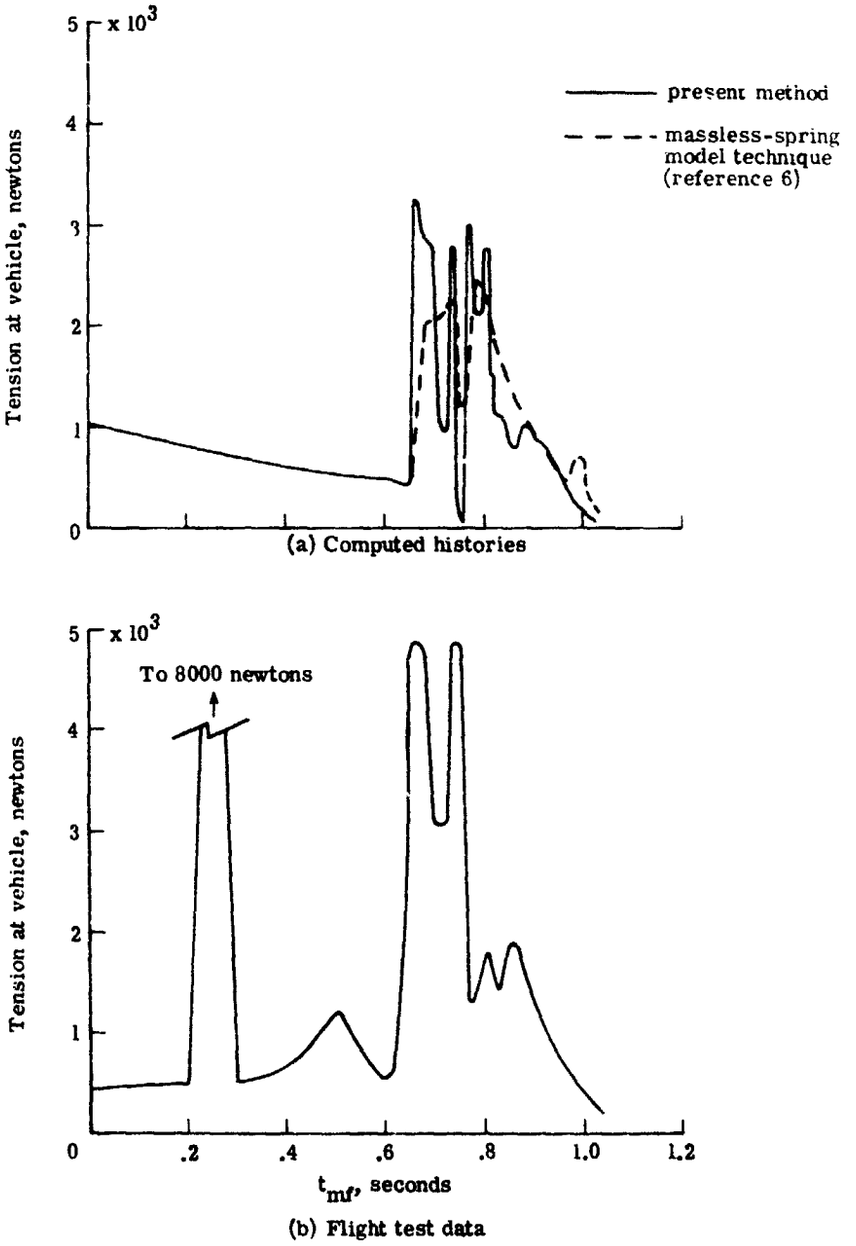

Figure 11.- Comparison of computed and flight-test histories of tension at vehicle during PEPP B/L-2 parachute deployment.

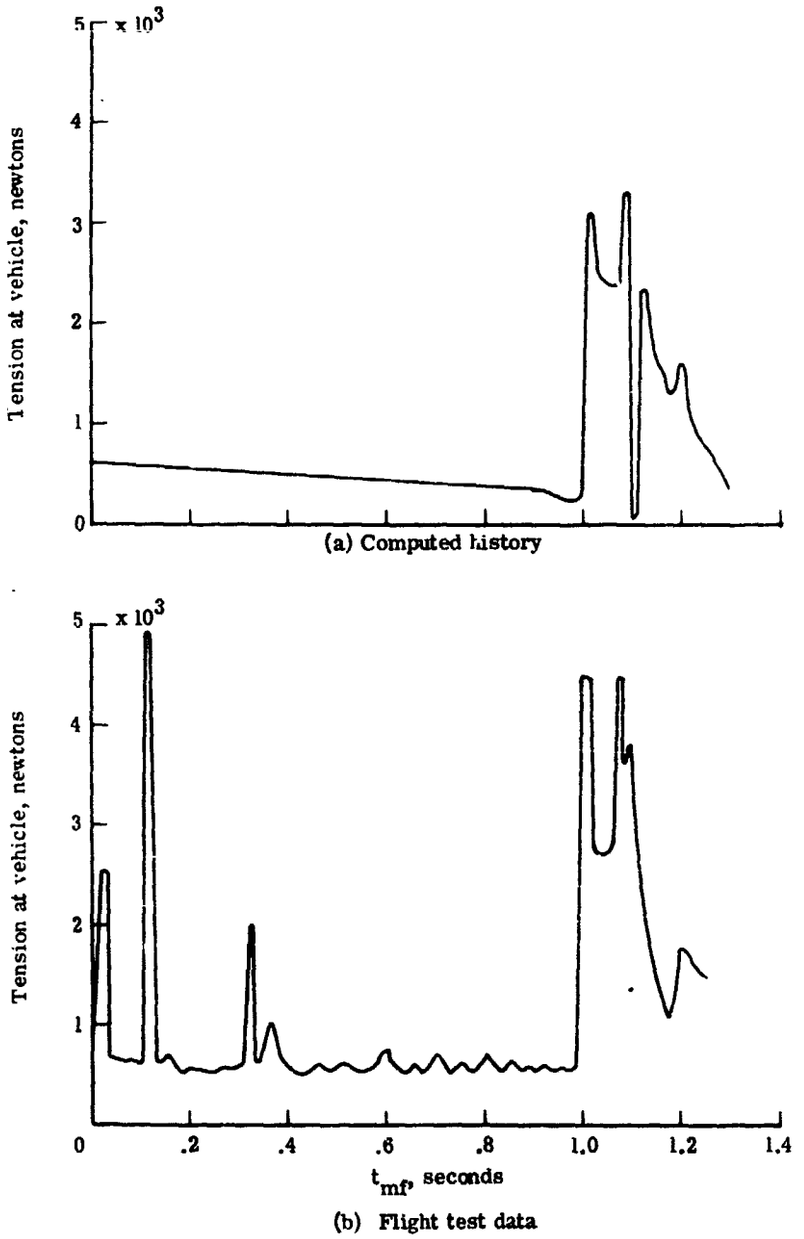

Figure 12.- Comparison of computed and flight-test histories of tension at vehicle during BLDT AV-4 parachute deployment.

mass density are encountered, the unfurling rate increases sharply. In comparing the computed B/L-2 unfurling rate history with the results presented in reference 6, it is evident that the magnitudes of the maxima and minima are decreased and increased, respectively, in the present history. Specifically, the unfurling rate as the gap portion of the canopy emerges from the deployment bag exceeds the local relative bag velocity but does not exceed the B/L-2 flight-test mortar ejection velocity, as the results in reference 6 showed. Although there is an absence of data concerning unfurling rate, the magnitudes presented in the present paper are thought to be good approximations to the magnitudes experienced during the flight-test deployments being studied.

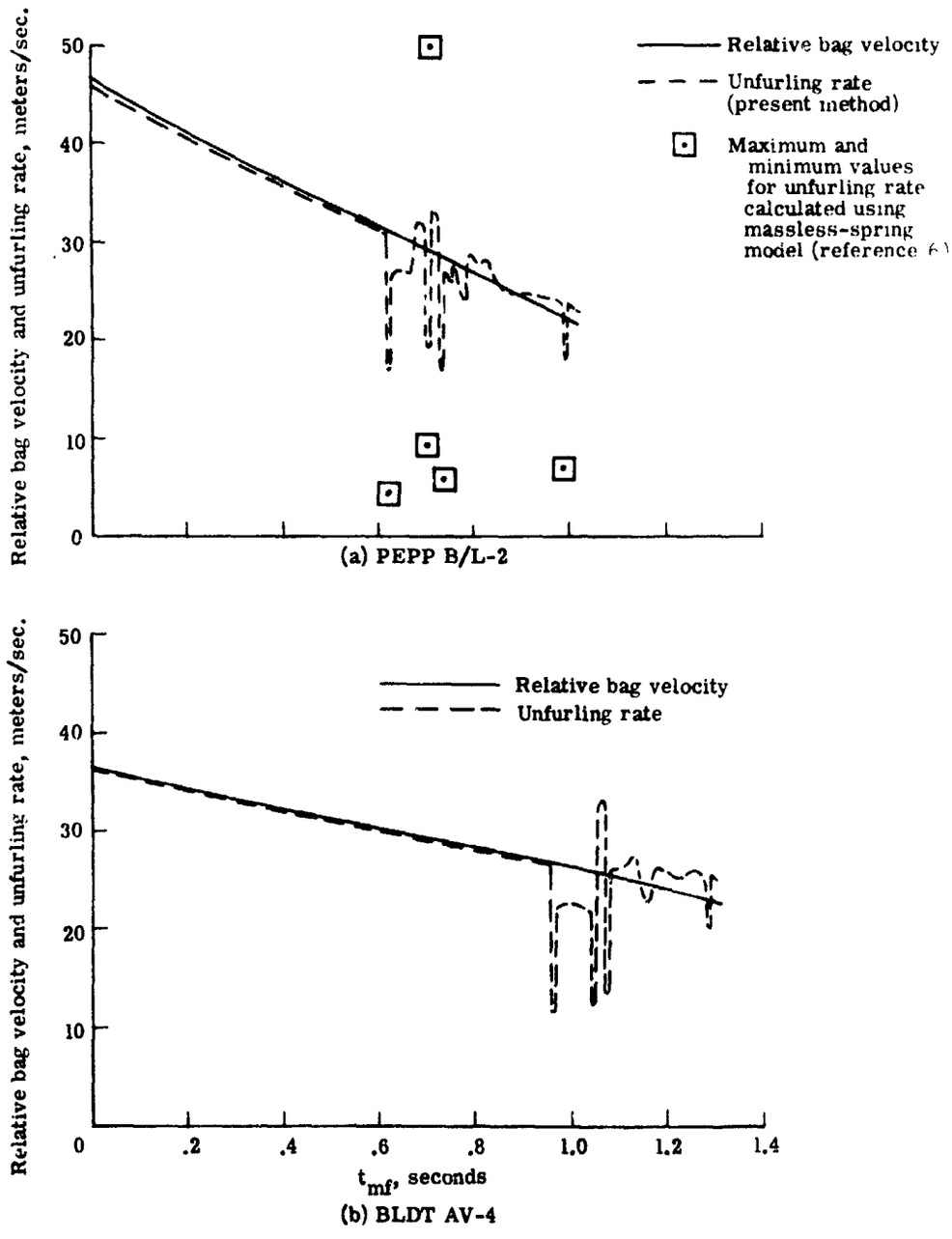

Figure 13.- Computed histories of relative bag velocity and unfurling rate for PEPP B/L-2 and BLDT AV-4.

CONCLUSIONS

The present paper has presented the equations governing the lines-first parachute unfurling process, including the equation and boundary conditions governing idealized longitudinal wave motion in the parachute suspension lines. Numerical techniques for obtaining a solution to the governing equations have been developed. Based on numerical solution of the governing equations for two disk-gap-band parachute deployment flight tests, the following conclusions can be made in evaluation of the present methods of simulation:

1. Computed histories of unfurled length agree very well with flight test data.
2. Computed histories of tension at the vehicle agreed well, in general, with flight test data histories. Errors in the computed histories were attributed to several areas of uncertainty, the most significant of which is probably a poorly defined boundary condition on the wave motion at the vehicle boundary.
3. Computed histories of unfurling rate exhibited fluctuation about the smooth histories of relative deployment bag velocity. However, the amplitudes of this fluctuation were attenuated as compared to the fluctuation experienced with the use of a massless-spring-type model of suspension-line elasticity. Specifically, no local values of unfurling rate computed using the present methods were observed to exceed the respective flight-test mortar ejection velocities. The

present computed histories are thought to be good approximations to the unfurling rates experienced during the flight tests being studied.

BIBLIOGRAPHY

1. Broderick, M. A.; and Turner, R. D.: Design Criteria and Techniques for Deployment and Inflation of Aerodynamic Drag Devices. ASD Tech. Rep. 61-88, U. S. Air Force, Nov. 1961.

2. Amer. Power Jet Co.: Performance of and Design Criteria for Deployable Aerodynamic Decelerators. ASD-TR-61-579, U. S. Air Force, Dec. 1963.

3. Huckins, Earle K., III: Techniques for Selection and Analysis of Parachute Deployment Systems. NASA TN D-5619, 1970.

4. Preisser, John S.; and Greene, George C.: Effect of Suspension Line Elasticity on Parachute Loads. J. Spacecraft and Rockets, vol. 7, no. 10, Oct. 1970, pp. 1278-1280.

5. Huckins, Earle K. III: A New Technique for Predicting the Snatch Force Generated During Lines-First Deployment of an Aerodynamic Decelerator. AIAA Paper No. 70-1171, Sept. 1970.

6. Poole, Lamont R.; and Huckins, Earle K. III: Evaluation of Massless-Spring Modeling of Suspension-Line Elasticity During the Parachute Unfurling Process. NASA TN D-6671, 1972.

7. Crandall, Stephen H.: Engineering Analysis. McGraw-Hill Book Co., Inc., 1956.

8. Bendura, Richard J.; Huckins, Earle K. III; and Coltrane, Lucille C.: Performance of a 19.7-Meter-Diameter Disk-Gap-Band Parachute in a Simulated Martian Environment. NASA TM X-1499, 1968.

9. Dickinson, D.; Schlemmer, J.; Hicks, F.; Michel, F.; and Moog, R. D.: Balloon-Launched Decelerator Test Program Post-Flight Test Report, BLDT Vehicle AV-4. NASA CR-112179, 1972.

10. Anon: U. S. Standard Atmosphere, 1962. NASA, U. S. Air Force, and U. S. Weather Bur., Dec. 1962.

11. Darnell, Wayne L.; Henning, Allen B.; and Lundstrom, Reginald R.: Flight Test of a 15-Foot Diameter (4.6 Meter) 120° Conical Spacecraft Simulating Parachute Deployment in a Mars Atmosphere. NASA TN D-4266, 1967.

12. Brown, Clarence A.; and Campbell, James F.: Evaluation of Flow Properties Behind 120° - and 140°-Included-Angle Cones and A Viking '75 Entry Vehicle at Mach Numbers from 1.60 to 3.95. NASA TN D-7089, 1973.

13. Hoerner, Sighard F.: Fluid-Dynamic Drag, published by Sighard F. Hoerner, 1958.

14. Lemke, Reinhold A.; Moroney, Richard D.; Nicuum, Ronald J.; and euhaus, Theodore J.: 65-Foot Diameter DGB Parachute, Planetary Entry Parachute Program. NASA CR-66589, 1967.

APPENDIX

PEPP B/L-2 AND BLDT AV-4 SYSTEM DESCRIPTIONS AND FLIGHT TEST DEPLOYMENT CONDITIONS

Proper simulation of the PEPP B/L-2 and BLDT AV-4 flight test deployment requires, of course, correct numerical input data. These data include mortar-fire trajectory conditions; vehicle mass, diameter, and aerodynamic characteristics; deployment bag mass, diameter, drag coefficient, and the velocity with which it is ejected by the mortar; parachute sizes and mass distributions; and suspension-line elastic characteristics. The data which were used to obtain the results presented in the present paper are described in this appendix.

Mortar-Fire Trajectory Conditions

Trajectory conditions at mortar fire for simulation of the two flight tests were selected so as to match the most important (with respect to the dynamics of the deployment process) variables, namely, the vehicle velocity v_v, the flight-path angle γ, and the freestream dynamic pressure q_∞. Values of these initial parameters are listed in references 8 and 9. The present simulation technique utilizes tables of atmospheric data from the U. S. Standard Atmosphere, 1962 (reference 10). Atmospheric data obtained prior to each of the flight tests were noticed to deviate slightly from those of the Standard Atmosphere. These deviations were taken into account by adjusting the input values for altitude at mortar fire downward to values at

which the tabular densities matched those local data values obtained prior to the flight tests. Mortar-fire trajectory parameters which were used in the simulation are listed in Table I.

TABLE I

INPUT TRAJECTORY CONDITIONS AT MORTAR-FIRE

	PEPP B/L-2	BLDT AV-4
Altitude, h, kilometers	39.8	44.4
Vehicle velocity, v_v, meters/second	518	698
Freestream dynamic pressure, q_∞, newtons/meter^2	555	522
Mach number	1.63	2.13
Flight-path angle, γ, degrees	50	12

Vehicle Descriptions

The B/L-2 flight test vehicle consisted of a 120°-included-angle cone aeroshell which enclosed a cylindrical payload. Mass, diameter, and drag characteristics (as a function of Mach number) for this vehicle were obtained from reference 11. The AV-4 flight test vehicle was a full-scale model of the Viking '75 entry vehicle. Mass, diameter, and drag characteristics for this vehicle were obtained from reference 9. As the flight test Mach numbers for B/L-2 and AV-4 varied only slightly during the unfurling process, the respective drag coefficients can be approximated by constants (see Table II). Tables of the wake parameter η as a function of distance aft of the vehicle bases were calculated using flow properties (namely, dynamic pressure and flow velocity) at the center of the wake of the two vehicles, which are presented in reference 12. The wake parameter

varies from a value of 0 at the base of the vehicle to values near 0.75 in the region of the wakes in which bag strip occurs. Vehicle masses, diameters, and approximate drag coefficients are summarized in Table II.

TABLE II

VEHICLE PHYSICAL CHARACTERISTICS AND DRAG COEFFICIENTS

	PEPP B/L-2	BLDT AV-4
Reference diameter, meters	4.6	3.5
Mass, m_v, kilograms	566	817
Approximate drag coefficient, $C_{D,v}$	1.5	1.6

Deployment-Bag Characteristics and Mortar Ejection Velocities

The parachutes for the respective flight tests were pressure-packed into cylindrical fabric deployment bags. Approximate bag masses were obtained from references 8 and 9. The bag diameter for each flight test was taken to be 0.3 meters. Drag coefficients for the bags were assumed to be constant and equal to 0.8, which is the approximate drag coefficient of a cylinder in uniform axial flow (reference 13). The unfurling resistance force F_{re} was determined in laboratory tests to be equal to an essentially constant value during the suspension-line unfurling phase and another essentially constant value during the canopy unfurling phase. Mortar ejection velocities were determined parametrically as those values required to obtain agreement between computed and flight-test data times from mortar fire to line stretch. These values, along with the previously mentioned deployment bag characteristics, are summarized in Table III.

TABLE III

DEPLOYMENT BAG CHARACTERISTICS

AND MORTAR EJECTION VELOCITIES

	PEPP B/L-2	BLDT AV-4
Mass, kilograms	0.9	0.8
Diameter, meters	.3	.3
Drag coefficient, $C_{D,b}$	.8	.8
Suspension-line unfurling resistance force, newtons	8.9	8.9
Canopy unfurling resistance force, newtons	26.7	26.7
Mortar ejection velocities, meters/second	46.4	36.6

Parachute Configurations

The PEPP B/L-2 flight test parachute was a disk-gap-band configuration having a nominal diameter of 19.7 meters. The linear-mass-density distribution for this parachute was calculated from detailed construction diagrams which are given in reference 14. This calculated mass distribution, for which it is assumed that the suspension system consists of suspension lines only, is shown in figure 14a. The BLDT AV-4 flight test parachute was also a disk-gap-band configuration and had a nominal diameter of 16.15 meters. The linear-mass-density distribution for this parachute was calculated from unpublished detailed construction blueprints. Figure 14b shows the calculated AV-4 distribution. The spikes in the calculated mass distributions denote areas in which there are several overlapped layers of canopy

cloth and a layer of fabric tape sewn onto the cloth layers around the circumference of that canopy section for reinforcement purposes. In the present solution method, these spikes are approximated by half-sine curves which attain the appropriate maximum amplitude at the mid-points of the spikes. Physical characteristics of the two parachutes which are used in the present simulation are summarized in Table IV.

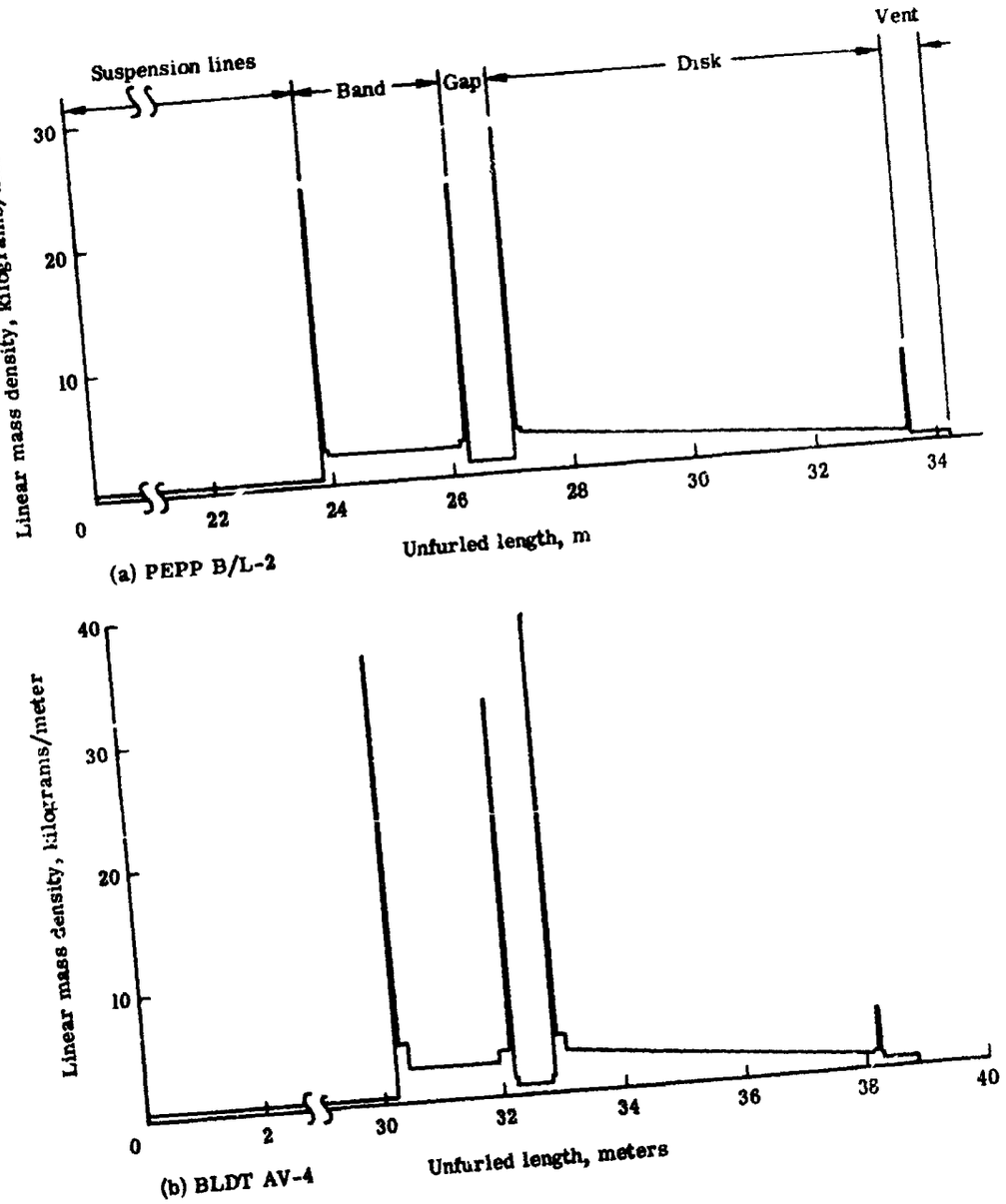

Figure 14.- Parachute linear-mass-density distributions.

TABLE IV

PHYSICAL CHARACTERISTICS OF PARACHUTES

	PEPP B/L-2	BLDT AV-4
Nominal diameter, meters	19.7	16.15
Number of suspension lines, n_{sl}	72	48
Total mass, kilograms	32.4	36.6
Suspension-line length, L_{sl}, meters	23.8	30.1
Total unfurled length of parachute, L_p, meters	34.3	38.8

Suspension-Line Elastic Characteristics

Suspension lines for the PEPP B/L-2 parachute were fabricated from coreless braided dacron cord having a rated tensile strength of 2450 newtons. Suspension lines for the BLDT AV-4 parachute were fabricated from similar cord having a rated tensile strength of 3900 newtons. Force-strain curves for representative samples of each type cord were obtained in laboratory tests using an Instron tensile-testing machine at a near-zero strain rate. These curves are shown in figure 15. A value of suspension-line damping coefficient was determined parametrically. As the tension at the vehicle never became zero during either of the flight-test deployments being studied, the damping coefficient was selected as that value required to maintain tension at the vehicle during both of the computed deployment histories.

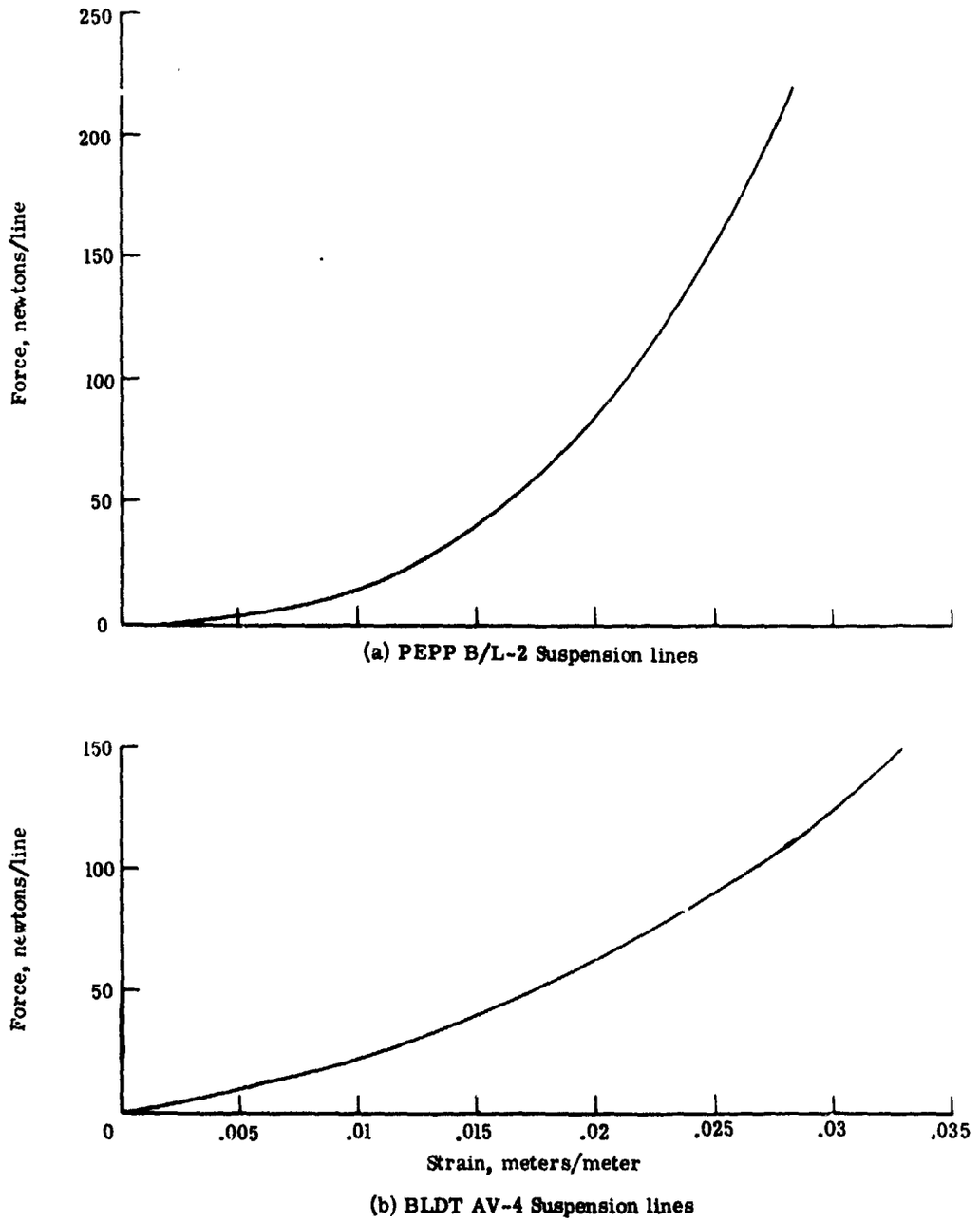

Figure 15.- Force-strain curves for parachute suspension lines.

Those particular values were determined to be 0.0465 N-sec/line for PEPP B/L-2 and 0.07 N-sec/line for BLDT AV-4.